Plume and Nanoparticle Formation During Laser Ablation

KW Kolasinski, West Chester University, West Chester, PA, United States
MC Gupta and LV Zhigilei, University of Virginia, Charlottesville, VA, United States

Glossary

Coulomb explosion Rapid particle escape driven by the buildup of like charges that repel each other.

Short-pulsed laser A laser with pulse duration in the range 1–30 ns.

Spallation The process in which separation and ejection of a molten or solid layer is driven by the relaxation of photomechanical stresses; it often proceeds through nucleation, growth and coalescence of multiple voids in a subsurface region of an ablation target.

Two-temperature model (TTM) A model of energy transfer that explicitly takes into account the different timescales for electron–electron energy transfer and electron–phonon energy transfer, which results in different temperature for electrons and the lattice on an ultrafast timescale.

**Ultrafast-pulsed laser** A laser with pulse duration ≤ 10 ps.

Nomenclature

d_{therm}	Thermal diffusion length
F	Laser fluence, often given in J cm^{-2}
MALDI	Matrix-assisted laser desorption/ionization
ML	Monolayer
p^*	Equilibrium vapor pressure
T_b	Normal boiling temperature
α	Absorption coefficient
κ	Thermal diffusivity
λ	Laser wavelength
τ_p	Laser pulse length

Introduction

Laser irradiation can lead to the formation of laser-induced periodic surface structures (LIPSS)[1–4] by a variety of mechanisms that remove or displace surface material. Irradiation that is sufficiently strong to induce melting can reshape a substrate surface through a variety of mechanisms including solidification-driven extrusion, hydrodynamics sputtering, capillary wave formation, the Mullins-Sekerka instability and laser zone texturing.[5]

Laser ablation is characterized by the explosive release of material from an irradiated target. The ablation process can be used to micromachine the target.[6–11] The formation of pillars during laser ablation just above the ablation threshold is a widely observed phenomenon. Mazur and coworkers[12] observed that reflectivity of silicon could be reduced across the whole of the visible and IR spectrum by the formation of laser ablation pillars. The formation of black silicon[13,14] is of great interest in photonic and photovoltaic applications. Indeed, the ability of laser ablation to change the reflectivity and color of not only silicon but also metal surfaces is a general phenomenon.[15,16] The nano-/microstructures formed by laser ablation can be replicated by transfer to a polymer mold.[17] Laser irradiation can also be used to remove tissue and control of biological cell growth.[18] Beginning in the 1980s, lasers were routinely used for ophthalmic dissection and ablation procedures. Its use soon spread to other medical subspecialties.[19]
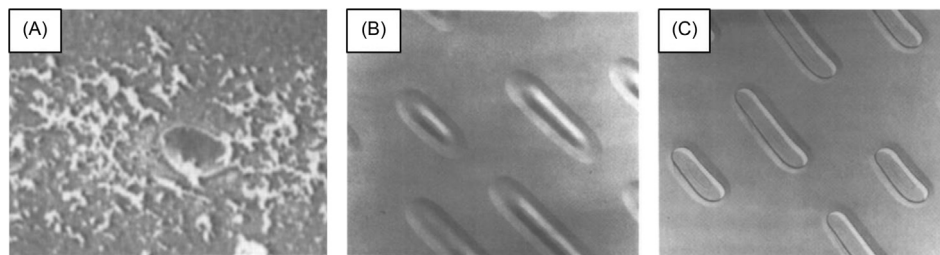
Fig. 1 Nanosecond pulse laser-generated marks on organic thin film without (A) and with (B, C) a transparent SiO$_2$ thin-film overcoat confining the flow of molten material. The marks generated without the confining overcoat, shown in (A), are irregularly decorated with ablation debris. Panel (B) is an image where the *top* overcoat film confines the molten material and the overcoat film is still present. Panel (C) shows the laser-generated marks after the overcoat film was removed after laser processing. There is no particulate formation in (B) and (C), while the laser-written marks on the thin film are still clearly visible. Reproduced with permission from Gupta, M. C. A Study of Laser Marking of Thin-Films, *J. Mater. Res.* **1988**, *3*, 1187–1195.

The material removed from the target can also be of interest. Shortly after lasers were first fired at targets, it was realized that the ejected material could be deposited into thin films in a controllable fashion.[20–23] Famously, Kroto, Heath, O'Brien, Curl and Smalley discovered C$_{60}$ (Buckminsterfullerene) by examining the products created by laser ablation of graphite,[24] which touched off a new frontier in carbon nanomaterials and led to the award of the Nobel Prize in Chemistry for three of the authors. Laser ablation is being used for solar cell manufacturing applications.[25,26] It is now widely recognized that laser ablation into vacuum, ambient gas or liquid can be used in a controlled fashion to make nanoparticles, which, under the proper conditions, exhibit not only a desired composition but also a narrow size distribution.[27–30] Laser ablation of, for example, Si or Ge in the presence of a metal catalyst can lead to the growth of nanowires.[31]

The morphology of the irradiated and ablated target can be exploited for controlled marking of the target. During the laser ablation process, nanoparticles and small clusters are formed along with particulates made of large clusters and droplets. The size of the particulate debris may vary from nanometers to microns. Depending on the application, the generation of particulates may be undesirable for laser micromachining and deposition of thin films. **Fig. 1A** shows a scanning electron microscope (SEM) image of laser-generated particulates observed on the substrate surface after ablation of an organic film.[32] Similar observations have been reported for metals, insulators, and semiconductors.[33] As will be discussed further, particulate density and size will vary with the incident laser energy density, laser pulse width, wavelength, melt viscosity, initial surface roughness and surrounding gas pressure. Odachi et al.[34] and Sharma et al.,[35] for example, have reported results on debris formation during femtosecond laser ablation of crystalline silicon and fused silica. Femtosecond laser irradiation mostly generates finer particles of less than 150 nm and wool-like debris which contain nanoparticles of silicon and SiO$_2$. There are significant differences in debris formation during ablation with nanosecond as opposed to ultrashort pulsed lasers with pico-to-femtosecond pulse durations due to high peak power and shorter laser interaction times. In the sections to follow, we discuss how photomechanical spallation and explosive boiling can lead to the ejection of molten material and particulate formation.

The pulsed laser-generated plume can be controlled by several means other than variation of the laser irradiation parameters. One method that will be discussed further below is control via the gas-phase composition and pressure. Another method that is particularly suitable for minimizing laser-generated debris in marking applications, such as that observed in **Fig. 1A**, is to overcoat the substrate with a transparent overlayer.[32,36,37] When laser ablation occurs, the overcoated film confines the plume and laser-generated molten material.[37] This completely suppresses formation of laser-generated particulates. **Fig. 1B** and **C** shows SEM images of a laser-marked organic thin film, which had been coated with a transparent SiO$_2$ layer prior to ablation. No debris is observed on the surface. Instead, only uniform and clearly discernable marks remain.

In this article, we concentrate on the mechanisms that create the plume of material ejected from a target due to its irradiation with short (nanosecond) or ultrafast (picosecond and femtosecond) pulsed lasers. The subsequent dynamics of the plume expansion and its role in the generation and transport of nanoparticles is also discussed. The perspective will mainly be that of irradiation of semiconductors and metals near and just above the ablation threshold with infrared, visible and near-UV lasers. Much of the discussion, however, is also relevant to molecular materials,[19,38] which are of particular interest, for example, in applications such as laser surgery, processing of polymeric materials, and matrix-assisted laser desorption/ionization (MALDI).

Short Pulse Ablation

We begin our discussion from irradiation with short-pulsed lasers by which we mean nanosecond (perhaps even to $\geq$ 150 ps) pulsed lasers. Commonly encountered lasers in this realm are Nd:YAG solid state and fiber (operating at 1064, 532 or

355 nm most commonly), and excimer lasers such as XeF (351 nm), XeCl (308 nm), KrF (248 nm), and ArF (193 nm). Incident photons are absorbed by the target and excite the electrons. Compared to the timescale of short pulses, the excited electrons rapidly transfer their energy to the lattice. Thus, the temperature of the electrons and phonons remains the same throughout the pulse. It is also important that, for strongly absorbing materials, the mechanical relaxation of a region heated by laser irradiation occurs on a timescale of tens of picoseconds,[39] that is, the irradiated area is able to expand during the short-pulse irradiation and to relieve much of the stress that would otherwise accumulate in the excited volume. For metals (and similarly for semiconductors much above their direct gap energy), the optical penetration depth is only 10–20 nm. Below bandgap irradiation of a semiconductor, for example, Si irradiated at a wavelength longer than roughly 350 nm for direct excitation, the laser penetration depth becomes longer and exhibits strong wavelength dependence. The length scale for thermal diffusion during the laser pulse, d_{therm}, is given by

$$d_{therm} = \sqrt{\kappa \tau_p} \qquad (1)$$

where κ is the thermal diffusivity and τ_p is the pulse length. At high temperatures, the thermal diffusivity ranges from about 2×10^{-5} m^2 s^{-1} for Fe to about 1×10^{-4} m^2 s^{-1} for Cu. Thus, the thermal diffusion length ranges from ~ 300 nm to ~ 700 nm over the course of a 5-ns pulse. These estimates are consistent with, for example, the results of Pedraza et al.,[40] who used the material parameters provided in Ref.[41] to estimate that irradiation of Si with 248 nm photons from a KrF laser with a pulse length of 25 ns and a fluence of 3 J cm^{-2} created a melt depth of ~ 1 μm that lasted for 250 ns.

If the laser fluence is only sufficient to cause melting, a mechanical phenomenon known as hydrodynamic sputtering can occur.[5] When performed under well-controlled conditions, the hydrodynamic flow can be used for laser-induced forward transfer of liquid droplets.[42] As an initially flat molten layer contracts in an attempt to lower its surface energy, the system evolves into a hemisphere if the process is slow enough. However, when the initial velocity of the layer is high, a liquid jet disintegrating into individual droplets may be ejected from the surface. The direction taken by the ejected fluid can be controlled to some degree by modifying the wetting properties, that is, contact angle, and the initial geometry of the fluid.[43]

Miotello and Kelly[44,45] performed critical analysis of three types of thermal processes that may be responsible for material loss during laser ablation: (a) normal vaporization from the irradiated surface, (b) heterogeneous bubble nucleation resulting from normal boiling in a zone extending from the surface to a depth defined the absorption length and/or the thermal diffusion length d_{therm}, and (c) homogeneous bubble nucleation leading to phase explosion (also called explosive boiling). Below, we briefly consider these three possibilities.

As radiant energy is dumped into the irradiated volume, it will heat the solid. Sublimation of a solid, which corresponds to the desorption of atoms/molecules from the surface of the solid, exhibits a rate R_{sub} that increases exponentially with temperature T according to

$$R_{sub} = \sigma A \exp(-\Delta H_{m,sub}/RT) \qquad (2)$$

where A is a preexponential factor, $\Delta H_{m,sub}$ is the molar enthalpy of sublimation (approximately equal to the sum of the molar enthalpies of fusion $\Delta H_{m,fus}$ and vaporization $\Delta H_{m,vap}$), T is the temperature and R is the gas constant. Since solids have a surface density of atoms of $\sigma \approx 10^{19}$ m^{-2} ($=1$ monolayer$=1$ ML) and a "usual" preexponential factor is $A \approx 10^{13}$ s^{-1}, we can expect the rate of sublimation to exhibit zero-order kinetics (the surface area is constantly replenished) with a value $\sigma A \approx 10^{13}$ ML s^{-1}. However, the thermal energy will diffuse out of the irradiated volume in several hundreds of nanoseconds. For a material such as Si, for which $\Delta H_{m,sub} \approx \Delta H_{m,fus} + \Delta H_{m,vap} \approx 50$ kJ mol^{-1} $+ 359$ kJ mol^{-1} ≈ 409 kJ mol^{-1}, we can estimate that even if the solid would be kept at its melting point of $T_m = 1683$ K for 1 μs, only 2×10^{-6} ML would desorb. If sufficient energy is deposited to melt the solid, then the activation energy in Eq. (2) becomes $\Delta H_{m,vap}$. Nonetheless, a liquid held at its melting point for 1 μs would only lose 7×10^{-5} ML and one held at its boiling point of $T_b = 2628$ K for 1 μs would lose only 0.7 ML. Therefore, thermal evaporation is of no consequence for short-pulse laser ablation compared to the loss of tens or even hundreds of nanometers per pulse that is commonly observed in laser ablation.

Concerning the second thermal mechanism, Miotello and Kelly[45] have shown that normal boiling with heterogeneous bubble formation is subject to a major kinetic bottleneck in the process of bubble diffusion. The formation and release of a bubble from the liquid/solid interface at the bottom of the region melted by laser irradiation is so slow that it will simply not occur on a timescale of less than 100 ns. This is because the value of the bubble diffusion coefficient leads to distances travelled that are atomically small for both 1 and 100 ns even at twice the melting temperature.

This leaves only phase explosion as a viable explanation for the efficient removal of material by short-pulse laser ablation. Phase explosion can be understood in simplified terms with the help of the diagram shown in Fig. 2, in which the reduced chemical potential $\mu/k_B T_c$, where T_c is the critical temperature and k_B is Boltzmann constant, is plotted versus reduced volume (V/V_c, where V_c is the critical volume). When the system is heated at equilibrium to its normal boiling temperature T_b, the liquid will be in contact with an equilibrium vapor pressure of $p^* = 101$ kPa. As the temperature increases, the equilibrium vapor pressure increases as well. Under these conditions, the liquid and vapor have equal chemical potential. When the material is rapidly heated by a laser pulse, however, the saturated vapor pressure does not have time to build up above the irradiated surface, and the liquid is brought to a metastable state, where the chemical potential of vapor is lower than that of the liquid. The metastable liquid does not instantaneously transform into a vapor because of the presence of a barrier separating the two states of the matter, $\Delta\mu^{\ddagger}$. As can be seen from Fig. 2, this
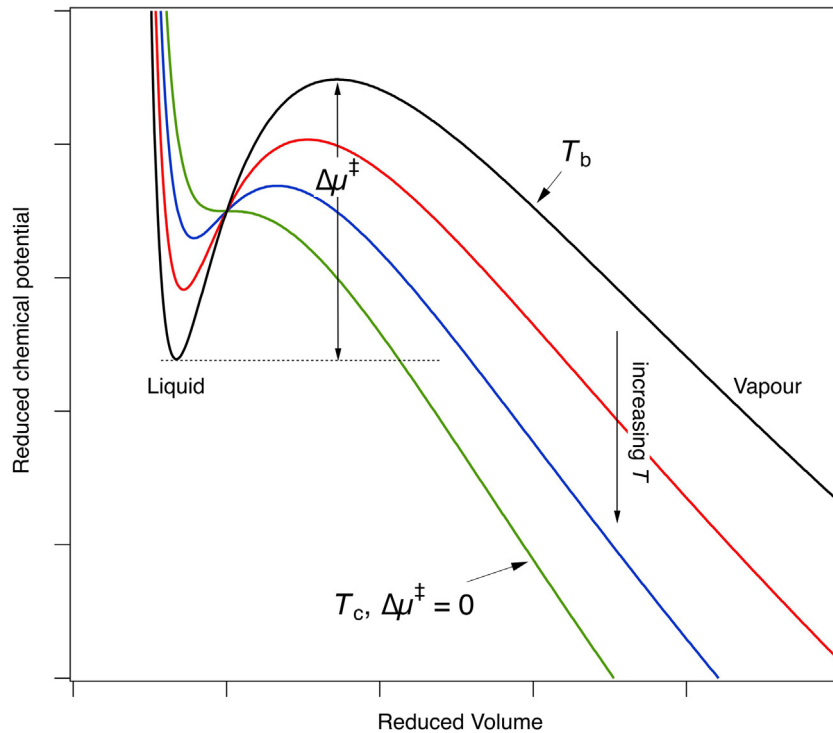
Fig. 2 The reduced chemical potential of a van der Waals fluid in the presence of saturation vapor pressure plotted as a function of reduced volume. The presence of a barrier $\Delta\mu^{\ddagger}$ separating the liquid and vapor states prevents the immediate transformation of a superheated liquid into vapor even in the presence of a strong thermodynamic driving force for the transformation.

barrier goes to zero at T_c, where the surface tension vanishes and the distinction between the liquid and vapor phases disappears. In a rapidly heated metastable system, however, this barrier vanishes at the spinodal temperature, T_{spin}, which is equal to the critical temperature T_c at the equilibrium pressure but is lower for the superheated/underpressured metastable liquid. A thermodynamic analysis based on classical nucleation theory reveals that, similarly to $\Delta\mu^{\ddagger}$, the barrier for the homogeneous nucleation of vapor bubbles in the metastable liquid decreases and the nucleation rate increases rapidly as the system approaches the spinodal line, which is invariably below T_c. As a result, one expects the onset of massive homogeneous nucleation of vapor phase (explosive boiling) at approximately 0.9 T_c.[44,45]

The evolution of the irradiated system can be understood as follows. As energy is transferred from the optical field to the sample, the temperature increases and the solid expands. Sublimation occurs but does not remove a substantial amount of material due to the short timescale. Further energy transfer increases the temperature to the melting point. After melting, which is occurring within the nanosecond pulse duration, evaporation takes place from the upper surface of the liquid, but this is not responsible for any significant material loss. Further energy deposition raises the temperature of the liquid, which is now expanding outward away from the bulk of the target. As the temperature reaches the threshold for the onset of the phase explosion, the superheated liquid is subject to spontaneous (explosive) release of vapor that drives rapid expansion of the material away from the irradiated target. This leads to the ejection of a mixture of vapor-phase atoms, atomic clusters and larger liquid droplets/nanoparticles. The formation of large liquid droplets is mainly coming from decomposition of a transient foamy structure generated in the slowly expanding lower part of the ablation plume.[39,46] It can be thought of in terms of nucleation, growth and percolation of multiple bubbles, as discussed in a theoretical treatment of Ref.[47] The relative fractions of the plume comprised of vapor, small clusters and larger droplets depend on the irradiation conditions and the composition of the target.

Expansion of the ejected material proceeds much like an adiabatic free jet expansion,[48,49] creating what is known as the laser ablation plume. The forward-directed nature of explosive evaporation results from anisotropic expansion velocities of different species, which are mainly controlled by the initial dimensions of the expanding plume. Collisions during the early stages of the expansion rapidly convert thermal energy into kinetic energy, which is mainly directed along the target normal at the initial stage of the plume expansion. High expansion velocities are attained which are rather uniform for all of the constituents of the plume. Collisions can also lead to changes in the fractions of atoms and clusters observed in the plume as condensation leads to further formation and growth of clusters. Evaporative cooling of clusters and droplets also occurs farther along the plume trajectory. The populations of different excited-state species in the plume is found to vary with distance away from the target.[50–53] The shape and temporal development of an ablation plume are exemplified in Fig. 3.
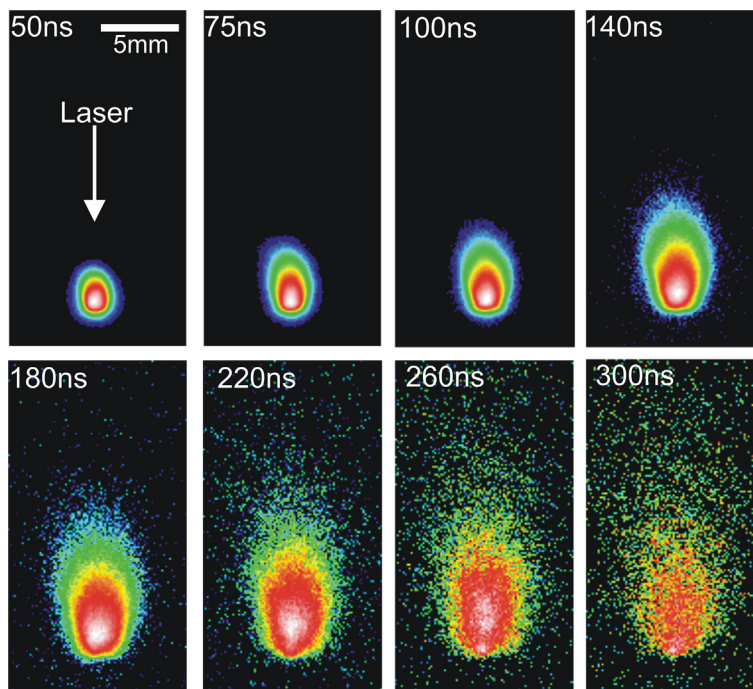
Fig. 3 The time evolution of visible emission from an aluminum plume recorded using an ICCD camera. The exposure time used was 2 ns. The laser power density of the Nd:YAG laser ($\tau_p = 8$ ns, $\lambda = 532$ nm) was 3 GW cm^{-2}, and background pressure was 1.3×10^{-4} Pa. The timings in the images represent the time after the onset of plasma formation. All of the images are normalized to their maximum intensity. Plume behavior indicates free expansion. Reproduced with permission from Harilal, S. S.; Bindhu, C. V.; Tillack, M. S.; Najmabadi, F.; Gaeris, A. C. Internal Structure and Expansion Dynamics of Laser Ablation Plumes Into Ambient Gases, *J. Appl. Phys.* **2003**, *93*, 2380–2388.

Condensation and cluster formation are enhanced if the ejected matter expands into an ambient gas with a pressure above ~ 10 Pa. Compared to the expansion into a vacuum, the interaction of the plume with an ambient gas is a far more complex gas dynamic process. The processes that occur include deceleration, attenuation, thermalization of the ablated species, diffusion, recombination, formation of shock waves, and chemical reactions, in addition to clustering.[54]

At a background pressure up to about 1 Pa, the plume expands freely. Up to about 10 Pa, there is strong interpenetration of the plume and the ambient gas. Above this pressure, collisions of the plume material with the ambient gas begin to change the nature of the plume expansion. A faster moving component is sometimes observed to split off from a slower moving component to cause plume splitting. Above 10 Pa, interpenetration falls off and a well-defined interface between plume and ambient gas forms. Along with deceleration, turbulence also appears in the expanding plume.

Cluster and nanoparticle formation are greatly enhanced by ablating a material into a moderate-pressure (10–1300 Pa) ambient gas. With increasing gas pressure, the film-deposition flux changes from primarily atoms and ions to clusters and nanoparticles. For example, Lowndes et al.[55] observed the deposition of 1–20 nm diameter Si nanoparticles onto Si substrates positioned 10–40 mm away from a Si wafer irradiated with ~ 1 J cm^{-2} of 193 nm light from an ArF excimer laser. Miotello and Patel[56] observed the deposition of both 11 ± 4 nm diameter (when observed with TEM) and 50–300 nm diameter (when observed at lower resolution with SEM) Co nanoparticles deposited into a B matrix when a pressed disk of cobalt–boron powder was ablated with a KrF excimer laser ($F = 3$ J cm^{-2}, $\lambda = 248$ nm). The cluster size/nanoparticle distribution depends not only on laser parameters (primarily τ_p, λ, and F) and ambient gas pressure but also the composition of the gas (He vs. Ar, or inert vs. reactive) and how the particles are collected. If they are collected onto a solid substrate, the distance to the substrate, its chemical composition and whether it is heated are important. The plume can also be collected by entraining it into a flow of gas that passes through a filter.

Laser ablation with ns-pulsed lasers is complicated by the fact that plume formation occurs during the laser pulse.[57] When the laser light is absorbed by the plume, the plume becomes highly ionized. A plasma strongly absorbs light and will shield the target from further irradiation. Strong laser–plasma interaction creates an additional high-pressure/high-energy region fueling expansion of the plume. As the plasma expands, the temperature drops very rapidly over the first 100 ns; however, the drop is smaller at later times (> 100 ns) because energy is regained in the recombination of ions.[54] The plume is also responsible for high recoil pressure exerted on the molten pool formed within the laser spot, which enhances ejection of material but also lowers the quality of laser drilling due to rim formation and splatter.

Ultrafast Ablation

While electron equilibration time is on the order of tens to hundreds of femtoseconds, the electron–phonon coupling time is typically on the order of picoseconds. This led Anisimov to develop the two-temperature model (TTM)[58] for the description of ultrafast excitations of metals. Two temperatures are required to describe the irradiated area because the electrons excited by a femtosecond laser pulse first equilibrate among themselves to attain a temperature T_e. On a much slower timescale, the energy of the excited electrons is transferred to the lattice, which is described by the temperature T_l.

Direct application of Eq. (1) yields the thermal diffusion length of only 10 nm for a 1-ps pulse, which is comparable to the penetration depth of light into a metal (the ballistic energy transfer by hot electrons may increase the effective depth of the energy deposition up to ∼100 nm in metals with low electron scattering rates[59, 60]). Furthermore, plume formation is significantly slower than the pulse duration. Therefore, no shielding of the incident radiation by plume absorption occurs.

Because of these factors, several characteristics of laser ablation change in the ultrafast regime. Short-pulse laser systems with $\tau_p \geq 1$ ns melt a significant amount of material that either does not leave the target in the first place, moves under hydrodynamic flow or is redeposited. Nanosecond ablation is always accompanied by the formation of a large heat-affected zone outside of the irradiated area. This limits the achievable precision and the quality of the structures created with nanosecond-pulsed lasers. On the other hand, ultrafast-pulsed laser ablation ($\tau_p < 10$ ps) exhibits a much shallower melting depth and smaller heat-affected zone. The material removal is more efficient for ultrafast ablation, for example, the ablation threshold is lowered and more material is ejected for the same fluence. A logarithmic dependence with either one[61] or two[62] thresholds is found, as exemplified for the latter case in Fig. 4.

In Fig. 4, the ablation depth per pulse L for laser fluences $F < 0.5$ J cm^{-2} is described by the expression

$$L \cong \alpha^{-1} \ln\left(F/F_{\text{th},\alpha}\right) \tag{3}$$

where α^{-1} is the optical penetration depth and $F_{\text{th},\alpha}$ is the threshold fluence for the ablation onset. A logarithmic fit to the experimental data gives $F_{\text{th},\alpha} = 140$ mJ cm^{-2} and $\alpha^{-1} = 10$ nm. This value for the optical penetration depth is in good agreement with $\alpha^{-1} = 13$ nm for Cu at a wavelength of 780 nm. This regime is only observed for subpicosecond pulses.

At higher fluences $F > 0.7$ J cm^{-2}, a second logarithmic dependence is observed,

$$L \cong l^{-1} \ln\left(F/F_{\text{th},l}\right) \tag{4}$$

This regime is characterized by the higher energy penetration depth $l = 80$ nm and higher threshold fluence $F_{\text{th},l} = 460$ mJ cm^{-2}. In this regime, only minor variations of the ablation depth per pulse are observed over the pulse durations ranging from 500 fs to 4.8 ps.

The explanation of two logarithmic dependences for subpicosecond-pulse laser ablation is somewhat controversial. Nolte et al. explained it on the basis of the optical penetration depth and the electron heat conduction.[62] They argue that, at low fluences, the density of hot electrons is low enough so that the energy transfer out of the optical penetration depth is negligible. Therefore, the optical penetration depth determines the length scale in the ablation depth versus fluence plot. For higher fluences, the electronic heat conduction is important and the second logarithmic dependence is found. The electronic heat diffusion occurs too rapidly for the first (low-fluence) regime to be observed with pulses longer than 1 ps.
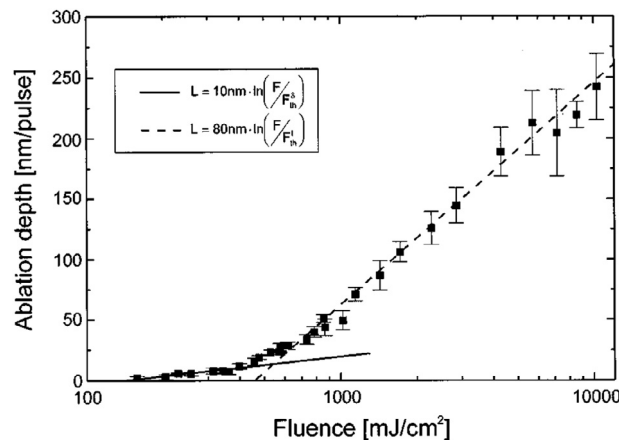
Fig. 4 Ablation depth per pulse versus fluence for Ti:sapphire ($\tau_p = 150$ fs, $\lambda = 800$ nm) irradiation of Cu. Two thresholds of 140 mJ cm^{-2} and 460 mJ cm^{-2} are found. Reproduced with permission from Nolte, S.; Momma, C.; Jacobs, H.; Tunnermann, A.; Chichkov, B. N.; Wellegehausen, B.; Welling, H.; Ablation of Metals by Ultrashort Laser Pulses, *J. Opt. Soc. Am. B: Opt. Phys.* **1997**, *14*, 2716–2722.

However, the results of detailed molecular dynamics (MD) simulations[38, 39, 46, 63–65] suggest a more nuanced explanation. The model applied to metals[46, 63–65] combines the MD method with a continuum description of laser excitation, electron–phonon equilibration and electron heat conduction. The simulations reveal the important role of photomechanical effects in defining the low-fluence threshold for the material ejection. The ultrafast ablation occurs not only in the regime of thermal confinement, but also under mechanical stress confinement, when the time of the laser heating is shorter than the time needed for the material expansion. As a result, the heating takes place under almost constant volume conditions and leads to the generation of strong compressive stresses. The mechanical action induced by the dynamic stress relaxation can lead to the separation and ejection of (usually molten) layer/droplets from the target. This mechanism of material ejection is commonly referred to as spallation[65] that proceeds through nucleation, growth, and coalescence of multiple voids in a subsurface region of an irradiated target. (For clarity, we only discuss spallation in the context of ultrafast excitation, where it is most frequently encountered. However, the occurrence of spallation depends on the laser penetration depth. When it is large (e.g., micrometers or longer—as in biological tissue or Si irradiated at photon energies below the bandgap), the stress confinement and spallation can play a role in nanosecond laser ablation as well.)

The spalled layer is unstable with respect to decomposition into droplets/nanoparticles, and as a result, the ablation yield in the spallation regime is characterized by a large mass fraction of large particulates and a minor presence of atoms or small clusters. As the fluence increases above the spallation threshold, the thickness of the spalled layer decreases until it finally vanishes with the emergence of phase explosion.[46]

A possible explanation for the occurrence of the second threshold for high-yield laser ablation—the fast rising curve in **Fig. 4**—is the combined effects of the phase explosion and melt expulsion due to the recoil pressure exerted by the ablation plume. Upon increase in the fluence of ultrafast irradiation beyond the threshold for phase explosion, the proportion of plume fraction composed of atoms and small clusters increases. The exact proportions depend on the irradiation conditions as well as the target material. For example, Barcikowski et al.[30] performed laser ablation experiments in air with eight different materials using a Ti:sapphire laser ($\tau_p = 120$ fs, $\lambda = 800$ nm, 1 mJ per pulse, 1 kHz repetition rate). They have shown that ablated graphite and Mg produce the highest percentage of nanoparticles (95–98%). Under identical conditions, Au and Ag aerosols are characterized by a significantly lower fraction of nanoparticles (15–25%).

In the subnanosecond regime, the pulse duration strongly affects the yield.[62, 63] Shorter pulses generally exhibit a higher yield. By comparing results of the simulations performed with 1 ps versus 50 ps excitation, it was found that stress confinement is responsible for the enhanced yield with shorter pulses because stress release synergistically contributes to the material ejection during phase explosion. Thus, both stress confinement and a lack of plume-induced shielding favor higher yields for ultrafast irradiation compared to longer pulse irradiation.

The environment above the target plays a strong role in ablation yield and plume dynamics. Femtosecond laser ablation in a gaseous environment is characterized by an up-to-10-times-higher ablation rate compared to laser ablation in water.[30] Despite much lower production rates, laser ablation in water and aqueous solutions allows for greater ability to manipulate the size, size dispersion and other properties of the nanoparticles. In particular, ablation at the liquid/solid interface can be used to synthesize nanoparticles with a small mean size and low size dispersion and to form ultrapure colloidal nanoparticles without using any chemical precursors or additives.

As revealed by the simulations of Wu and Zhigilei,[46] the yield of species in the plume varies with size. Small atomic clusters and larger droplets are predicted to exhibit power-law size distributions, with clusters and droplets characterized by different power law exponents in the range -1.4 to -2.3. Interestingly, a simplified Monte Carlo modeling of the phase explosion by considering rapid nucleation and growth of vapor bubbles also predicts a power-law size distribution of droplets with similar values of the power-law exponent.[47]

It should be recognized that a Gaussian laser intensity profile—as is usually encountered for most lasers other than excimer lasers—means that the central more intense portion of the beam may activate the phase explosion mechanism, while the lower intensity wings are simultaneously capable of inducing spallation. A composite schematic from Ref.[46] of all the processes occurring during ultrafast ablation above the spallation and ablation thresholds is shown in **Fig. 5**.

The greater excitation density of ultrafast ablation, as alluded to above, leads to a potentially increased importance for nonthermal ejection mechanisms. Indeed, evidence shows that nonthermal pathways do make a measurable contribution, even if it is not the predominant mechanism of material ejection. It has been argued[66] that Coulomb explosion (or a related process) is observed, if the laser energy is deposited in a very short time, perhaps 20–200 fs depending on the material. A signature of this mechanism is the emission of particles with kinetic energies as high as several eV. While no evidence of nonthermal ejection with 248 nm ns pulses was found, Henley et al.[52] observed evidence of nonthermal ejection of C from graphite with fs pulses, and Bashir et al.[66] observed hyperthermal Si atoms emitted from Si(111) wafers irradiated by Ti:sapphire laser ($\tau_p = 25$ fs, $\lambda = 800$ nm). Coulomb explosion is more likely in insulators, for UV irradiation or for extremely intense ultrafast irradiation, during which multiphoton or high-field effects start to play a role.[20] Indeed, it has been shown theoretically[67] that the Coulomb explosion can be activated in wide-bandgap dielectrics, where laser-induced electron photoemission can produce positive charge accumulation up to the level sufficient for disintegration of a surface layer of the target by electrostatic repulsive forces. In semiconductors and metals, on the other hand, the high mobilities of charge carriers prevent the charge accumulation and make the Coulomb explosion unlikely.
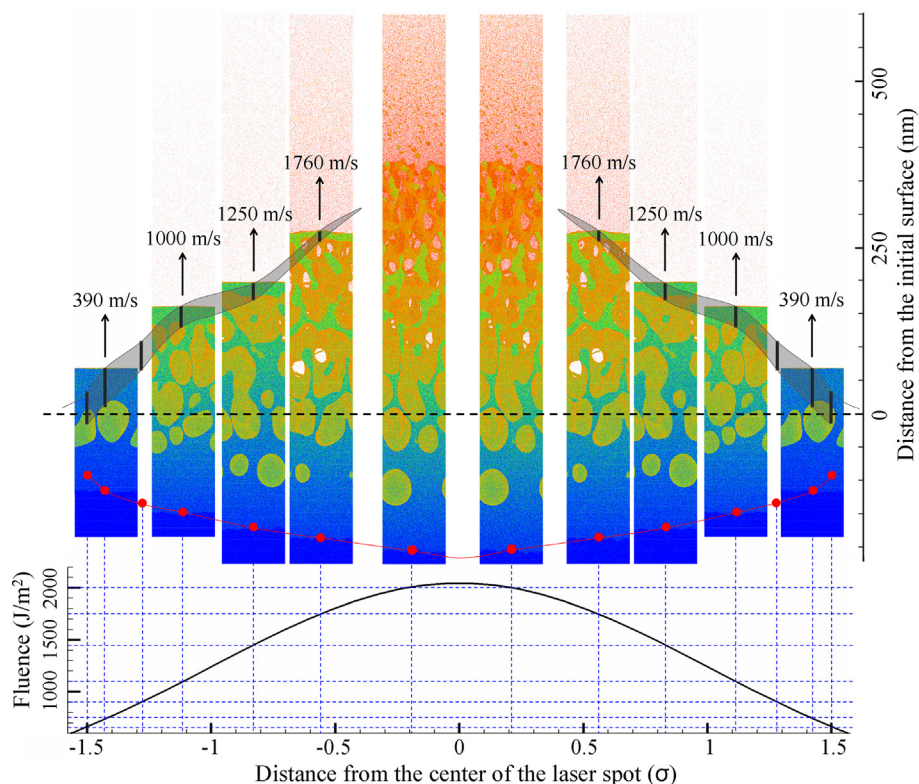
Fig. 5 The integral visual picture of melting, generation of subsurface voids, and material ejection from an Al target irradiated by a 100-fs laser pulse. The laser beam has a Gaussian spatial profile with a peak absorbed laser fluence of 2050 J m^{-2}, as shown in the bottom part of the figure. The representation of the laser-induced processes at the scale of the whole laser spot is based on a "mosaic approach," where snapshots from individual TTM-MD simulations taken at the same time of 150 ps after the laser pulse are aligned with locations within the laser spot that correspond to the values of local fluence used in the simulations, as shown by the thin vertical and horizontal dashed lines. The atoms in the snapshots are colored by their potential energy, from blue for low energy atoms in the bulk of the target to red for the vapor-phase atoms. The red dots connected by the red line mark the location of the melting front. The thicknesses and locations of the top void-free layers are shown by black bars for simulations performed in the spallation regime and, in the case of the lowest fluence of 650 J m^{-2}, just below the spallation threshold. For two local fluences, 650 and 900 J m^{-2}, the locations of the melting front and the void-free layers are marked without showing the corresponding snapshots. The velocities of the *top* void-free layers at 150 ps are provided in the figure. Reproduced with permission from Wu, C. P.; Zhigilei, L. V.; Microscopic Mechanisms of Laser Spallation and Ablation of Metal Targets From Large-Scale Molecular Dynamics Simulations, *Appl. Phys. A* **2014**, *114*, 11–32.

Conclusions

A plume of atoms, small clusters, and nanoparticles is formed during laser ablation. Especially at gas pressures above 10 Pa or for irradiation into liquids, the plume provides a ready source of nanoparticles. The size distribution of the nanoparticles can be controlled by adjusting both the irradiation parameters and the characteristics of the substrate onto which they are collected and the environment around it. The primary mechanism of material removal during laser ablation—for both nanosecond and ultrafast pulsed irradiation—is phase explosion. As the temperature of the solid approaches the spinodal temperature, the expanding heated layer spontaneously decomposes into a mixture of vapor-phase atoms and liquid droplets. For ultrafast irradiation, an additional ablation mechanism is the photomechanical spallation, which may lead to the ejection of liquid layer and droplets below the threshold for the phase explosion. Laser ablation is highly prized for its ability to produce films that are structured over the nano- and mesoscales on both the irradiated target and the substrate that is used to collect material from the ablation plume.

See also: Interaction of Ultrafast Laser Pulses With Nanostructure Surfaces; Laser-Induced Processes in Thin Ices; The Chemomechanical Modification of Silicon with Macroscopic Diamond Tips and AFM Tips with Extension to Laser-Modification of the Material, Starting from Its Roots in Monolayers on Hydrogen-Terminated Silicon.

References

1. Sipe, J. E.; Young, J. F.; Preston, J. S.; Van Driel, H. M. Laser-Induced Periodic Surface-Structure. I. Theory. *Phys. Rev. B* **1983,** *27,* 1141–1154.
2. Young, J. F.; Preston, J. S.; van Driel, H. M.; Sipe, J. E. Laser-Induced Periodic Surface Structure. II. Experiments on Ge, Si, Al, and Brass. *Phys. Rev. B* **1983,** *27,* 1155–1172.
3. Young, J. F.; Sipe, J. E.; Van Driel, H. M. Laser-Induced Periodic Surface-Structure. III. Fluence Regimes, the Role of Feedback, and Details of the Induced Topography in Germanium. *Phys. Rev. B* **1984,** *30,* 2001–2015.
4. Siegman, A. E.; Fauchet, P. M. Stimulated Wood's Anomalies on Laser-Illuminated Surfaces. *IEEE J. Quantum Electron.* **1986,** *22,* 1384–1403.
5. Kolasinski, K. W. Solid Structure Formation During the Liquid/Solid Phase Transition. *Curr. Opin. Solid State Mater. Sci.* **2007,** *11,* 76–85.
6. Vorobyev, A. Y.; Guo, C. L. Direct Femtosecond Laser Surface Nano/Microstructuring and Its Applications. *Laser Photonics Rev.* **2013,** *7,* 385–407.
7. Tan, B.; Venkatakrishnan, K. A Femtosecond Laser-Induced Periodical Surface Structure on Crystalline Silicon. *J. Micromech. Microeng.* **2006,** *16,* 1080–1085.
8. Hwang, D. J.; Grigoropoulos, C. P.; Choi, T. Y. Efficiency of Silicon Micromachining by Femtosecond Laser Pulses in Ambient Air. *J. Appl. Phys.* **2006,** *99,* 083101.
9. Dickinson, J. T. Physical and Chemical Aspects of Laser-Materials Interactions. In *Photon-Based Nanoscience and Nanobiotechnology;* Dubowski, J. J., Tanev, S., Eds., Springer: Dordrecht, 2006; pp 1–30.
10. Oliveira, V.; Conde, O.; Vilar, R. UV Laser Micromachining of Ceramic Materials: Formation of Columnar Topographies. *Adv. Eng. Mater.* **2001,** *33,* 75–81.
11. Mishra, S.; Yadava, V. Laser Beam MicroMachining (LBMM)—A Review. *Opt. Lasers Eng.* **2015,** *73,* 89–122.
12. Her, T.-H.; Finlay, R. J.; Wu, C.; Deliwala, S.; Mazur, E. Microstructuring of Silicon With Femtosecond Laser Pulses. *Appl. Phys. Lett.* **1998,** *73,* 1673–1675.
13. Otto, M.; Algasinger, M.; Branz, H.; Gesemann, B.; Gimpel, T.; Fuechsel, K.; Kaesebier, T.; Kontermann, S.; Koynov, S.; Li, X. P.; Naumann, V.; Oh, J.; Sprafke, A. N.; Ziegler, J.; Zilk, M.; Wehrspohn, R. B. Black Silicon Photovoltaics. *Adv. Opt. Mater.* **2015,** *3,* 147–164.
14. Liu, X. G.; Coxon, P. R.; Peters, M.; Hoex, B.; Cole, J. M.; Fray, D. J. Black Silicon: Fabrication Methods, Properties and Solar Energy Applications. *Energy Environ. Sci.* **2014,** *7,* 3223–3263.
15. Vorobyev, A. Y.; Guo, C. L. Colorizing Metals With Femtosecond Laser Pulses. *Appl. Phys. Lett.* **2008,** *92,* 041914.
16. Nayak, B. K.; Gupta, M. C.; Kolasinski, K. W. Formation of Nano-textured Conical Microstructures in Titanium Metal Surface by Femtosecond Laser Irradiation. *Appl. Phys. A* **2008,** *90,* 399–402.
17. Caffrey, P. O.; Nayak, B. K.; Gupta, M. C. Ultrafast Laser-Induced Microstructure/Nanostructure Replication and Optical Properties. *Appl. Opt.* **2012,** *51,* 604–609.
18. Bush, J. R.; Nayak, B. K.; Nair, L. S.; Gupta, M. C.; Laurencin, C. T. Improved Bio-implant Using Ultrafast Laser Induced Self-assembled Nanotexture in Titanium. *J. Biomed. Mater. Res. B Appl. Biomater.* **2011,** *97b,* 299–305.
19. Vogel, A.; Venugopalan, V. Mechanisms of Pulsed Laser Ablation of Biological Tissues. *Chem. Rev.* **2003,** *103,* 577–644.
20. Balling, P.; Schou, J. Femtosecond-Laser Ablation Dynamics of Dielectrics: Basics and Applications for Thin Films. *Rep. Prog. Phys.* **2013,** *76,* 036502.
21. Willmott, P. R.; Huber, J. R. Pulsed Laser Vaporization and Deposition. *Rev. Mod. Phys.* **2000,** *72,* 315–328.
22. Bäuerle, D. *Laser Processing and Chemistry,* 3rd ed.; Springer-Verlag: Berlin, 2000.
23. Chrisey, D. B.; Hubler, G. K. *Pulsed Laser Deposition of Thin Films,* Wiley: New York, 1994.
24. Kroto, H. W.; Heath, J. R.; O'Brien, S. C.; Curl, R. F.; Smalley, R. E. C_{60}: Buckminsterfullerene. *Nature (London)* **1985,** *318,* 162–163.
25. Petridis, C.; Savva, K.; Kymakis, E.; Stratakis, E. Laser Generated Nanoparticles Based Photovoltaics. *J. Colloid Interface Sci.* **2017,** *489,* 28–37.
26. Dahlinger, M.; Carstens, K.; Hoffmann, E.; Zapf-Gottwick, R.; Werner, J. H. 23.2% Laser Processed Back Contact Solar Cell: Fabrication, Characterization and Modeling. *Prog. Photovolt.* **2017,** *25,* 192–200.
27. Semaltianos, N. G. Nanoparticles by Laser Ablation. *Crit. Rev. Solid State Mater. Sci.* **2010,** *35,* 105–124.
28. Perrière, J.; Boulmer-Leborgne, C.; Benzerga, R.; Tricot, S. Nanoparticle Formation by Femtosecond Laser Ablation. *J. Phys. D. Appl. Phys.* **2007,** *40,* 7069–7076.
29. Zhang, D.; Gökce, B.; Barcikowski, S. Laser Synthesis and Processing of Colloids: Fundamentals and Applications. *Chem. Rev.* **2017,** *117,* 3990–4103.
30. Barcikowski, S.; Hahn, A.; Kabashin, A. V.; Chichkov, B. N. Properties of Nanoparticles Generated During Femtosecond Laser Machining in Air and Water. *Appl. Phys. A* **2007,** *87,* 47–55.
31. Morales, A. M.; Lieber, C. M. A Laser Ablation Method for the Synthesis of Crystalline Semiconductor Nanowires. *Science* **1998,** *279,* 208–211.
32. Gupta, M. C. A Study of Laser Marking of Thin-Films. *J. Mater. Res.* **1988,** *3,* 1187–1195.
33. Siew, W. O.; Lee, W. K.; Wong, H. Y.; Yong, T. K.; Yap, S. S.; Tou, T. Y. Investigation of Droplet Formation in Pulsed Nd: YAG Laser Deposition of Metals and Silicon. *Appl. Phys. A* **2010,** *101,* 627–632.
34. Odachi, G.; Sakamoto, R.; Hara, K.; Yagi, T. Effect of Air on Debris Formation in Femtosecond Laser Ablation of Crystalline Si. *Appl. Surf. Sci.* **2013,** *282,* 525–530.
35. Sharma, S. P.; Oliveira, V.; Vilar, R. Morphology and Structure of Particles Produced by Femtosecond Laser Ablation of Fused Silica. *Appl. Phys. A* **2016,** *122,* 261.
36. Klein-Wiele, J. H.; Simon, P. Sub-100 nm Pattern Generation by Laser Direct Writing Using a Confinement Layer. *Opt. Expr.* **2013,** *21,* 9017–9023.
37. Karim, E. T.; Shugaev, M.; Wu, C. P.; Lin, Z. B.; Hainsey, R. F.; Zhigilei, L. V. Atomistic Simulation Study of Short Pulse Laser Interactions With a Metal Target Under Conditions of Spatial Confinement by a Transparent Overlayer. *J. Appl. Phys.* **2014,** *115,* 183501.
38. Zhigilei, L. V.; Leveugle, E.; Garrison, B. J.; Yingling, Y. G.; Zeifman, M. I. Computer Simulations of Laser Ablation of Molecular Substrates. *Chem. Rev.* **2003,** *103,* 321–348.
39. Zhigilei, L. V. Dynamics of the Plume Formation and Parameters of the Ejected Clusters in Short-Pulse Laser Ablation. *Appl. Phys. A* **2003,** *76,* 339–350.
40. Pedraza, A. J.; Jesse, S.; Guan, Y. F.; Fowlkes, J. D. Laser-Induced Surface Perturbations in Silicon. *J. Mater. Res.* **2001,** *16,* 3599–3608.
41. de Unamuno, S.; Fogarassy, E. A Thermal Description of the Melting of C- and A-silicon Under Pulsed Excimer Lasers. *Appl. Surf. Sci.* **1989,** *36,* 1–11.
42. Willis, D. A.; Grosu, V. Microdroplet Deposition by Laser-Induced Forward Transfer. *Appl. Phys. Lett.* **2005,** *86,* 244103.
43. Afkhami, S.; Kondic, L. Numerical Simulation of Ejected Molten Metal Nanoparticles Liquefied by Laser Irradiation: Interplay of Geometry and Dewetting. *Phys. Rev. Lett.* **2013,** *111,* 034501.
44. Miotello, A.; Kelly, R. Critical Assessment of Thermal Models for Laser Sputtering at High Fluences. *Appl. Phys. Lett.* **1995,** *67,* 3535–3537.
45. Miotello, A.; Kelly, R. Laser-Induced Phase Explosion: New Physical Problems When a Condensed Phase Approaches the Thermodynamic Critical Temperature. *Appl. Phys. A* **1999,** *69,* S67–S73.
46. Wu, C. P.; Zhigilei, L. V. Microscopic Mechanisms of Laser Spallation and Ablation of Metal Targets From Large-Scale Molecular Dynamics Simulations. *Appl. Phys. A* **2014,** *114,* 11–32.
47. Mazzi, A.; Gorrini, F.; Miotello, A. Liquid Nanodroplet Formation Through Phase Explosion Mechanism in Laser-Irradiated Metal Targets. *Phys. Rev. E* **2015,** *92,* 031301.
48. Kelly, R.; Dreyfus, R. W. On the Effect of Knudsen-Layer Formation on Studies of Vaporization, Sputtering, and Desorption. *Surf. Sci.* **1988,** *198,* 263.
49. Scoles, G. *Atomic and Molecular Beam Methods*; Vol. 1; Oxford University Press: New York, 1988.
50. Jesse, S.; Pedraza, A. J.; Fowlkes, J. D.; Budai, J. D. Etching-Enhanced Ablation and the Formation of a Microstructure in Silicon by Laser Irradiation in an SF_6 Atmosphere. *J. Mater. Res.* **2002,** *17,* 1002–1012.
51. Claeyssens, F.; Henley, S. J.; Ashfold, M. N. R. Comparison of the Ablation Plumes Arising From ArF Laser Ablation of Graphite, Silicon, Copper, and Aluminum in Vacuum. *J. Appl. Phys.* **2003,** *94,* 2203–2211.
52. Henley, S. J.; Carey, J. D.; Silva, S. R. P.; Fuge, G. M.; Ashfold, M. N. R.; Anglos, D. Dynamics of Confined Plumes During Short and Ultrashort Pulsed Laser Ablation of Graphite. *Phys. Rev. B* **2005,** *72,* 205413.
53. Straw, M.; Randolph, S. Direct Spatiotemporal Analysis of Femtosecond Laser-Induced Plasma-Mediated Chemical Reactions. *Laser Phys. Lett.* **2014,** *11,* 035601.

54. Harilal, S. S.; Bindhu, C. V.; Tillack, M. S.; Najmabadi, F.; Gaeris, A. C. Internal Structure and Expansion Dynamics of Laser Ablation Plumes Into Ambient Gases. *J. Appl. Phys.* **2003,** *93,* 2380–2388.
55. Lowndes, D. H.; Rouleau, C. M.; Thundat, T.; Duscher, G.; Kenik, E. A.; Pennycook, S. J. Silicon and Zinc Telluride Nanoparticles Synthesized by Pulsed Laser Ablation: Size Distributions and Nanoscale Structure. *Appl. Surf. Sci.* **1998,** *127,* 355–361.
56. Miotello, A.; Patel, N. Pulsed Laser Deposition of Cluster-Assembled Films for Catalysis and the Photocatalysis Relevant to Energy and the Environment. *Appl. Surf. Sci.* **2013,** *278,* 19–25.
57. Lu, Q. Thermodynamic Evolution of Phase Explosion During High-Power Nanosecond Laser Ablation. *Phys. Rev. E* **2003,** *67,* 016410.
58. Anisimov, S. I.; Kapeliovitch, B. L.; Perel'man, T. L. Two Temperature Model. *Sov. Phys.–JETP* **1974,** *39,* 375.
59. Hohlfeld, J.; Wellershoff, S.-S.; Güdde, J.; Conrad, U.; Jähnke, V.; Matthias, E. Electron and Lattice Dynamics Following Optical Excitation of Metals. *Chem. Phys.* **2000,** *251,* 237–258.
60. Byskov-Nielsen, J.; Savolainen, J.-M.; Christensen, M. S.; Balling, P. Ultra-Short Pulse Laser Ablation of Copper, Silver and Tungsten: Experimental Data and Two-Temperature Model Simulations. *Appl. Phys. A* **2011,** *103,* 447–453.
61. Preuss, S.; Demchuk, A.; Stuke, M. Sub-Picosecond UV Laser Ablation of Metals. *Appl. Phys. A* **1995,** *61,* 33–37.
62. Nolte, S.; Momma, C.; Jacobs, H.; Tunnermann, A.; Chichkov, B. N.; Wellegehausen, B.; Welling, H. Ablation of Metals by Ultrashort Laser Pulses. *J. Opt. Soc. Am. B: Opt. Phys.* **1997,** *14,* 2716–2722.
63. Zhigilei, L. V.; Lin, Z. B.; Ivanov, D. S. Atomistic Modeling of Short Pulse Laser Ablation of Metals: Connections Between Melting, Spallation, and Phase Explosion. *J. Phys. Chem. C* **2009,** *113,* 11892–11906.
64. Ivanov, D. S.; Zhigilei, L. V. Kinetic Limit of Heterogeneous Melting in Metals. *Phys. Rev. Lett.* **2007,** *98,* 195701.
65. Leveugle, E.; Ivanov, D. S.; Zhigilei, L. V. Photomechanical Spallation of Molecular and Metal Targets: Molecular Dynamics Study. *Appl. Phys. A* **2004,** *79,* 1643–1655.
66. Bashir, S.; Rafique, M. S.; Husinsky, W. Surface Topography (Nano-sized Hillocks) and Particle Emission of Metals, Dielectrics and Semiconductors During Ultra-Short-Laser Ablation: Towards a Coherent Understanding of Relevant Processes. *Appl. Surf. Sci.* **2009,** *255,* 8372–8376.
67. Bulgakova, N. M.; Stoian, R.; Rosenfeld, A.; Hertel, I. V.; Campbell, E. E. B. Electronic Transport and Consequences for Material Removal in Ultrafast Pulsed Laser Ablation of Materials. *Phys. Rev. B* **2004,** *69,* 054102.

Further Reading

Anisimov, S. I.; Luk'yanchuk, B. S. Selected Problems of Laser Ablation Theory. *Physics-Uspekhi* **2002,** *45,* 293–324.

Kolasinski, K. W. Surface Science: Foundations of Catalysis and Nanoscience, 3rd ed.; Wiley: Chichester, 2012.